

# Absolute calibration of gravitational wave detector using gravity field and photon pressure

Yuki Inoue,<sup>1,2</sup> Sadakazu Haino,<sup>1,2</sup> Nobuyuki Kanda,<sup>3</sup> Yujiro Ogawa,<sup>2,4</sup> Toshikazu Suzuki,<sup>2,5,6</sup> Takayuki Tomaru,<sup>2,4,5,6</sup> Takahiro Yamanmoto,<sup>7</sup> and Takaaki Yokozawa<sup>7</sup>

<sup>1</sup>*Institute of Physics, Academia Sinica, Taipei 11529, Taiwan.*

<sup>2</sup>*High Energy Accelerator Research Organization (KEK), Ibaraki 305-0801, Japan*

<sup>3</sup>*Department of Physics, Graduate School of Science, Osaka City University, Osaka 558-8585, Japan*

<sup>4</sup>*The Graduate University for Advanced Studies,*

*Hayama, Miura District, Kanagawa 240-0115, Japan*

<sup>5</sup>*Kavli Institute for the Physics and Mathematics of the Universe (Kavli IPMU),*

*The University of Tokyo, Chiba 277-8568, Japan*

<sup>6</sup>*Institute for Cosmic Ray Research, The University of Tokyo, Chiba 277-8582, Japan*

<sup>7</sup>*Institute for Cosmic Ray Research, The University of Tokyo, Gifu 506-1205, Japan*

Absolute calibration of the gravitational wave detectors is an essential to evaluate the various parameters of the gravitational wave sources. The photon calibrator is primary calibrator for calibrating the absolute displacement of the mirror by using the photon pressure. Current technological limit of the absolute calibration uncertainty is 3.5 % corresponding to the uncertainty of the laser power standard of the standard metrology institutes from nine country. In order to reduce the uncertainty of the photon calibrator, we propose a new method using the combination of photon calibrator and gravity field calibrator. The gravity field calibrator gives the modulation to mirror using the gravity gradient. In previous study, uncertainty of the distance between the test mass and gravity field calibrator is one of the serious systematic error of the absolute calibration. To cancel this uncertainty, we newly propose the method of quadrupole and hexapole mass distribution. We also estimated the uncertainty of this method. The estimated precision of absolute calibration is 0.22%, which is 10 times less than that of previous method.

## I. INTRODUCTION

The discovery of the gravitational wave (GW) gave us the new probe for observing our universe [? ]. The typical strain sensitivity,  $h$ , of 2nd generation interferometric detectors (IFO), such as Advanced LIGO [? ], Advanced Virgo [? ], and KAGRA [? ? ], are around  $10^{-23}/\sqrt{\text{Hz}}$  at 100 Hz. By using the GW signals from compact binary coalescences, we can derive the parameters such as masses, spins, luminosity distance, orbital inclination and the sky location of the binary system from the detected waveforms. The precision of the derived parameters are potentially limited by the calibration accuracy. As the number of detected sources increases and we detect higher signal-to-noise ratio (SNR) events, the calibration uncertainty will become the dominant source of the errors to extract physics information. In particular, the uncertainty on the absolute GW signal amplitude directly propagates to the error on the estimation of the distance to the sources. The detection of GW signal from a Binary Neutron Star (BNS) system, GW170817 [? ] in both GW and Electro-Magnetic (EM) waves opened a new era of multi-messenger astronomy. These observations allow us to use GW170817 as a standard siren [? ? ? ? ] to determine the absolute luminosity distance to the source directly from the GW signal measurements. Assuming the event rate of  $3000 \text{ Gpc}^{-3}\text{yr}^{-1}$  which is consistent with the bounds from GW170817 at 90% confidence [? ], we expect to detect GW signals from about 50 BNS standard sirens in the next few observing runs. They can constrain the Hubble constant ( $H_0$ ) measure-

ment to 2% or less [? ], and eventually resolve the  $3\text{-}\sigma$  tension of the  $H_0$  measurement between Cepheid-SN distance ladder [? ] and CMB data assuming a  $\Lambda\text{CDM}$  model. [? ] The systematic errors on the calibration of the absolute GW signal amplitude must be suppressed at the sub-% level to achieve the high precision  $H_0$  measurement with the GW standard sirens.

An interferometer measures the change of distance difference along the two arms of interferometer. Then, the fluctuations in the degree of freedom of differential arm length (DARM) is suppressed by the DARM control loop. The reconstruction signal of DARM fluctuation at the observation frequency is excited by the gravitational waves. We can reconstruct the gravitational waveform with the calibrated error and control signals of this DARM loop. To calibrate the signals, the accurate modelings of the actuator and sensing function are essential. To understand the model, we need to measure the transfer function and monitor the time dependency of the transfer function using continuous sine curve (calibration lines). The residual of the time-dependent models corresponds to uncertainty of the detection.

To reduce the calibration systematic uncertainty, we need to inject well parameterized calibration line by photon calibrator (Pcal) or other calibration source for monitoring the time variation of the response of IFO. The first generation of the photon calibrator was developed by the Glasgow and GEO600 [? ? ]. They proposed the modulation method with photon pressure for understanding the response of interferometer. The second generation photon calibrator is developed by LIGO [? ? ? ? ].

LIGO and Virgo employ the second generation photon calibrator for the calibration of time-dependent response of IFO [? ]. The third generation photon calibrator is developed by KAGRA [? ]. KAGRA employ the 20 W laser and independent modulation system for injected beams. LIGO and KAGRA use a power sensor called to as the Gold standard, which is calibrated by the laser power standard of NIST in Boulder, CO [? ]. However, it has a challenging issue of the absolute calibration due to the accuracy of the absolute laser power of laser standard between national metrology institute from nine countries. The systematic discrepancies between nine countries are as large as 3.5 % [? ].

The dynamic gravity field calibrator (Gcal) is one of the candidates to be able to solve the uncertainty problem of absolute calibration. The technologies of the system are established and tested in Forward and Miller [? ], Weber [? ? ], University of Tokyo [? ? ? ? ? ] and Rome university group [? ]. Related techniques using gravity field calibrator for the calibration are discussed in Matone et al [? ]. It can modulate the test mass using gravity gradient with rotor. The amplitude of displacement of the mirror is determined by masses, distance, frequency, radius, and gravity constant.

In this paper, we propose how we can achieve sub-percent uncertainty of the calibration. We focus on the combination method of the photon calibrator and gravity field calibrator. In section II, we explain how to calibrate with photon calibrator. In chapter III, we show the principle of multipole moment gravity and modulation method. In section IV, we show how to calibrate the absolute displacement with Pcal and Gcal. In section V, we discuss the systematic error by changing parameters.

## II. PHOTON CALIBRATOR

Pcal relies on the photon radiation pressure from the power modulated laser beams reflecting on the test mass to apply periodic force via the recoil of photons [? ]. advanced LIGO, advanced Virgo and KAGRA employ the photon calibrator for the calibration of the interferometer response [? ? ? ]. Each gravitational detectors placed the 1047 nm laser around the end test mass. The displacement of the test mass can be described as

$$x = \frac{P \cos \theta}{2c} s(\omega) \left( 1 + \frac{M}{I} \vec{a} \cdot \vec{b} \right), \quad (1)$$

where  $P$  is absolute laser power,  $\theta$  is incident angle of the Pcal laser,  $M$  is mass of test mass,  $\omega$  is angular frequency of the laser power modulation,  $\vec{a}$  and  $\vec{b}$  are position vector of Pcal laser beams. The schematic view is shown in Fig. 1.  $I = Mh^2/12 + Mr^2/4$  is the moment of inertia, where  $h$  and  $r$  are thickness and radius of test mass.  $s(\omega)$  is transfer function between force and displacements. We can regard the  $s(\omega)$  as  $1/(M\omega^2)$  above 20 Hz.

The laser power is stabilized less than design sensitivity. The schematic view of the photon calibrator is shown

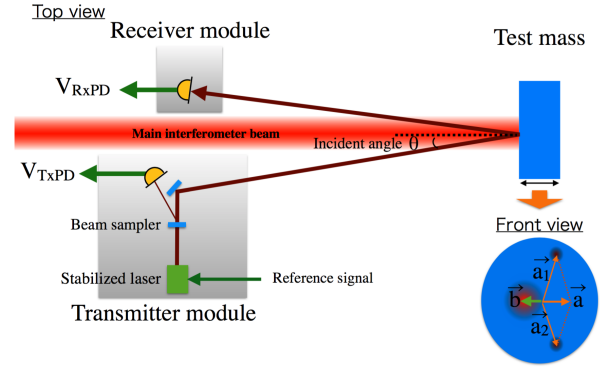


FIG. 1. Schematic view of photon calibrator. We place the stabilized laser on the transmitter module. The injected signal at the test masses is monitored by using the response of photo detector power between the transmitter module,  $V_{TxPD}$  and receiver module,  $V_{RxPD}$ . The geometrical factor is characterized by the position vectors of photon calibrator beams,  $\vec{a} = \vec{a}_1 + \vec{a}_2$ , and the main beam,  $\vec{b}$ .

in Fig. 1. The stabilized laser is mounted on the transmitter module. The power is monitored by the response of the photo detectors at the transmitter module,  $V_{TxPD}$ , and receiver module,  $V_{RxPD}$ . The largest relative uncertainty of photon calibrator is that of laser power. LIGO and KAGRA use the working standard to cross-calibrate the relative response of each interferometer. The relative uncertainty of each calibrator is 0.51 % [? ]. The second largest relative uncertainty is an optical efficiency of the optical path. We calibrate the injected power from the outside of the vacuum chamber. Therefore, we need to consider the optical efficiency due to the transmittance of the vacuum window and reflectance of the mirrors. The measured uncertainty of optical efficiency in LIGO is 0.37 %. For the absolute calibration, the detector, so called “Gold standard”, is calibrated with the NIST laser power standard. After that, the responses of “Working standard” of Hanford, Livingston and KAGRA are calibrated by the “Gold standard” in LIGO Hanford observatory. However, the result of comparison between accuracies of the absolute laser powers of each institutes has 3.5 % uncertainty. It implies that the serious systematic error for distance estimation because the uncertainty of the absolute calibration propagate to the distance of the GW source.

## III. GRAVITY FIELD CALIBRATOR

To solve the uncertainty problem of the absolute calibration, we propose the method of gravity field calibrator. The gravity field calibrator generate the dynamic gravity field at the end of test mass by rotating the multipole masses. The rotor placed in the vacuum chamber for isolating the acoustic noise. To monitor the frequency,

TABLE I. Specification summary of LIGO, Virgo and KAGRA photon calibrator

|                           | KAGRA    | advanced LIGO | advanced Virgo |
|---------------------------|----------|---------------|----------------|
| Mirror material           | Sapphire | Silica        | Silica         |
| Mirror mass               | 23 kg    | 40 kg         | 40 kg          |
| Mirror diameter           | 220 mm   | 340 mm        | 350 mm         |
| Mirror thickness          | 150 mm   | 200 mm        | 200 mm         |
| Distance of Pcal from ETM | 36 m     | 8 m           | 1.5 m          |
| Pcal laser power          | 20 W     | 2 W           | 3 W            |
| Pcal laser frequency      | 1047 nm  | 1047 nm       | 1047 nm        |
| Incident angle            | 0.72 deg | 8.75 deg      | 30 deg         |

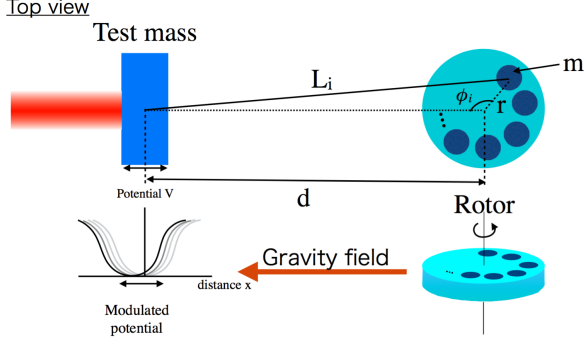


FIG. 2. Schematic view of gravity field calibrator. We placed the rotor at the same height and the distance of  $d$  away from test masses. Multipole mass generate the gravitational potential at the test mass position.

we mount the 10-bit encoder. We read the response of encoder using 16 bit ADC system. We calculated the displacement by changing dynamic gravity field of multipole moment with  $N$  peaces of masses. We assumed the suspended test mass for the interferometer and disk with multipole masses as shown in Fig 2. We put the masses,  $m$ , at the positions of the radius,  $r$ . The distance between the center of mass of mirror and disk is assumed  $d$ . We rotate the disk at the angular frequency of  $\omega_{\text{rot}} = 2\pi f_{\text{rot}}$ .

First we calculate the distance with  $N$  pieces of masses which are separated by radius of  $r$  from the center of the rotor mass and arranged at equal intervals, respectively. Distance between  $i$ -th mass and center of test mass is written as

$$L_i = d \sqrt{1 + \left(\frac{r}{d}\right)^2 - 2 \left(\frac{r}{d}\right) \cos \phi_i}, \quad (2)$$

where the angle of  $i$ -th mass is assumed as  $\phi_i = \omega_{\text{rot}} t + 2\pi i/N$ . The gravity potential at the center of test mass can be described as

$$V = \sum_{i=0}^N V_i \quad (3)$$

$$= -GMm \sum_{i=0}^N L_i^{-1} \quad (4)$$

$$= -\frac{GMm}{d} \sum_{i=0}^N \sum_{n=0}^{\infty} \left(\frac{r}{d}\right)^n P_n \left( \cos \left( \omega_{\text{rot}} t + \frac{2\pi i}{N} \right) \right), \quad (5)$$

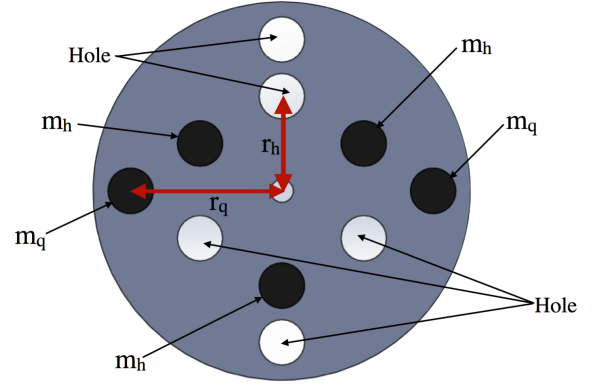


FIG. 3. Configuration of the rotor with quadrupole and hexapole mass distributions.  $m_q$  and  $m_h$  are masses of quadrupole and hexapole.  $r_q$  and  $r_h$  are radiuses of quadrupole and hexapole.

where  $P_n$  is Legendre polynomial, and  $V_i$  is potential of a mass. The equation of motion of test mass is

$$Ma = \left| \frac{\partial V}{\partial d} \right| = \frac{GMm}{d^2} \sum_{i=0}^N \sum_{n=0}^{\infty} (n+1) \left(\frac{r}{d}\right)^n \times P_n \left( \cos \left( \omega_{\text{rot}} t + \frac{2\pi i}{N} \right) \right), \quad (6)$$

where  $a$  is acceleration of test mass.

We place the quadrupole and hexapole masses in the same rotor as shown in Fig. 3. We put the hole between each mass. The hole can increase the gravity gradient twice effectively. Therefore, we can describe the equation of motion as

$$Ma = \left| \frac{\partial V}{\partial d} \right| = \frac{2GMm}{d^2} \sum_{i=0}^N \sum_{n=0}^{\infty} (n+1) \left(\frac{r}{d}\right)^n \times P_n \left( \cos \left( \omega_{\text{rot}} t + \frac{2\pi i}{N} \right) \right). \quad (7)$$

We will calculate the displacement of quadrupole and hexapole in the section III A and III B.

### A. Displacement of test mass (Quadrupole)

We calculate the displacement of the quadrupole masses distribution corresponding to  $N = 2$ . The masses and radiuses of quadrupole are assumed as  $m_q$  and  $r_q$ . The equation of motion of test mass is described as

$$Ma = \frac{2GMm_q}{d^2} \sum_{n=0}^{\infty} (n+1) \left(\frac{r_q}{d}\right)^n \times \sum_{i=0}^1 P_n (\cos (\omega_{\text{rot}} t + \pi i)). \quad (8)$$

If we assume  $r \ll d$ , the displacement of the time-dependent lower harmonics can be written by

$$x = \sum_{k=1}^{\infty} x_{kf} \cos(k\omega_{\text{rot}} t) \sim x_{2f} \cos(2\omega_{\text{rot}} t) = x_{2f} \cos \omega t, \quad (9)$$

where  $k$  is the number of the harmonics. The amplitude of 2-f rotation is described as

$$x_{2f} = 9 \frac{GMm_q r_q^2}{d^4} s(\omega). \quad (10)$$

### B. Displacement of test mass (Hexapole)

We also calculate the displacement of the hexapole masses distribution, which corresponds to  $N = 3$ . The masses and radiuses of hexapole are assumed as  $m_h$  and  $r_h$ . The equation of motion of test mass is described as

$$Ma = \frac{2GMm_h}{d^2} \sum_{n=0}^{\infty} (n+1) \left( \frac{r_h}{d} \right)^n \quad (11)$$

$$\times \sum_{i=0}^2 P_n \left( \cos \left( \omega_{\text{rot}} t + \frac{2\pi i}{3} \right) \right). \quad (12)$$

If we assume  $r \ll d$ , the displacement of the time-dependent lower harmonics can be written by

$$x = \sum_{k=1}^{\infty} x_{kf} \cos(k\omega_{\text{rot}} t) \sim x_{3f} \cos(3\omega_{\text{rot}} t) = x_{3f} \cos \omega t, \quad (13)$$

where amplitude of 3-f is described as

$$x_{3f} = 15 \frac{GMm_h r_h^3}{d^5} s(\omega). \quad (14)$$

## IV. ABSOLUTE POWER CALIBRATION BY USING GCAL AND PCAL

In this section, we discuss about absolute laser power calibration using interferometer. Figure 4 shows the configuration of the calibration by using the combination of photon calibrator and gravity field calibrator. First, we modulate the mirror position using gravity field calibrator. We can measure the signal of  $x_{2f}$  and  $x_{3f}$  in the response of interferometer. Second, we send the interferometer signal to the excitation port of photon calibrator as a reference signal port of feedback control as shown in Fig. 4. The photon calibrator cancel the displacement by gravity field calibrator. Third, we measure the response of the detector of transmitter module and receiver module, whose units are volt. The output signal of transmitter module,  $V_{\text{TxPD}}$  and receiver module,  $V_{\text{RxPD}}$  should be corresponding to displacement from gravity field. By using Eq (I),(10), and (14), the modulated powers are

$$P_{2f} = 18 \frac{Gcm_q Mr_q^2}{d^4 \cos \theta} \frac{1}{1 + \frac{M}{I} \vec{a} \cdot \vec{b}} \quad (15)$$

$$P_{3f} = 30 \frac{Gcm_h Mr_h^3}{d^5 \cos \theta} \frac{1}{1 + \frac{M}{I} \vec{a} \cdot \vec{b}} \quad (16)$$

Fourth, we demodulate the signal of the transmitter and receiver modules using the measured encoder signal of

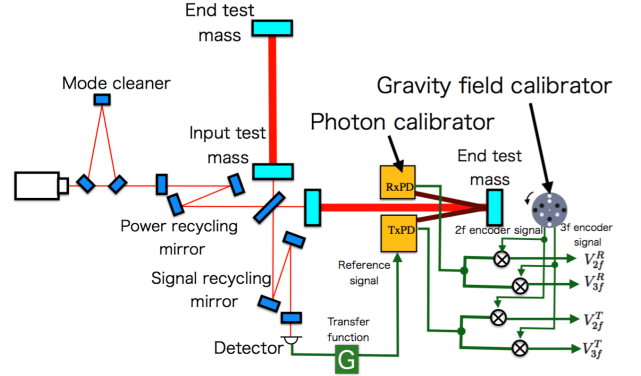


FIG. 4. Test setup of the absolute calibration. We place the gravity field calibrator behind of the test mass. The frequency of the gravity field calibrator is monitored by the encoder output. The error signal of differential arm length of the interferometer send to the reference port of the photon calibrator for canceling of the modulation of dynamic gravity field with feedback technique, where  $G$  is transfer function. Output signals from the photon calibrator are synchronized with the force from the gravity field calibrator. We demodulate the output signals by using 2-f and 3-f signal monitored by encoder.

gravity field calibrator. The demodulated signals are

$$V_{2f}^T = \rho_T P_{2f}, \quad (17)$$

$$V_{2f}^R = \rho_R P_{2f}, \quad (18)$$

$$V_{3f}^T = \rho_T P_{3f}, \quad (19)$$

$$V_{3f}^R = \rho_R P_{3f}, \quad (20)$$

where  $\rho_T$  and  $\rho_R$  are transfer function from power to voltage of the photo detector output at the transmitter and receiver modules. Therefore, we can measure the distance with the ratio of response between 2-f and 3-f components:

$$d = \frac{5}{3} \frac{V_{2f}^T}{V_{3f}^T} \frac{m_h}{m_q} \frac{r_h^3}{r_q^2} = \frac{5}{3} \frac{V_{2f}^R}{V_{3f}^R} \frac{m_h}{m_q} \frac{r_h^3}{r_q^2}. \quad (21)$$

Finally, we calculate the displacement formula of Pcal calibrated by Gcal. we insert the equation (10) to the Eq. (I):

$$x = \frac{P \cos \theta}{2c} s(\omega) \left( 1 + \frac{M}{I} \vec{a} \cdot \vec{b} \right) \quad (22)$$

$$= 9 \frac{Gm_q Mr_q^2}{d^4} \frac{P}{P_{2f}} s(\omega), \quad (23)$$

$$= \frac{729}{625} \frac{GMm_q^5 r_q^{10}}{m_h^4 r_h^{12}} \frac{V_{3f}^{R4}}{V_{2f}^{R5}} V_{\text{in}} s(\omega), \quad (24)$$

where we assume  $P(\omega) = \rho_R V_{\text{in}}$ , and  $V_{\text{in}}$  is amplitude of the input voltage.  $(GMm_q^5 r_q^{10})/(m_h^4 r_h^{12})$  は定数なので 予め測定を行う事が可能。  $V_{3f}^R/V_{2f}^R$  は上記のキャリブレーション作業で測定する。この測定は干渉系のレスポンス

TABLE II. The assumed parameters.  $G$  is gravity constant [ ].  $\theta$  is incident angle of the Pcal beam.  $M$  is mass of test mass.  $1 + \frac{I}{M} \vec{a} \cdot \vec{b}$  is geometrical factor.

|   | Value  | Relative uncertainty |
|---|--|----------------------|
| $G$                                     | $6.67408 \times 10^{-11} \text{ m}^3 \text{ kg}^{-1} \text{ sec}^{-2}$ | 0.0047 %             |
| $\cos \theta$                           | 1.000  | 0.07 %               |
| $M$                                     | 22.89 kg   | 0.02 %               |
| $m_q$                                   | 4.485 kg   | 0.004 %              |
| $m_h$                                   | 4.485 kg   | 0.004 %              |
| $r_q$                                   | 0.200 m  | 0.010 %              |
| $r_h$                                   | 0.125 m  | 0.016 %              |
| $1 + \frac{I}{M} \vec{a} \cdot \vec{b}$ | 1  | 0.3 %                |

の変化をモニターしながらはかる。LIGO の場合 Working standard を用いた Pcal のキャリブレーション作業を XX 頃に行っている。Gravity field calibrator は GS/WS 作業に対応するものなので、同程度かそれ以上の頻度でオペレーションすべきであろう。したがって、Gcal は干渉系の operation 時に動かさなくて良いことを言及しておく。これまでの Study では reconstruction を考慮に入れた Gcal のオペレーションが提案されていたが、この方法は Pcal で Reconstruction をおこなう。その理由は PCal の有する広い周波数でのオペレーションを応用できるからである。Gcal をの振幅を変化させる事は難しいが、AOM ではそれらを自由に变化できる。また、オペレーション時に Gcal を運用するとアコースティックノイズや地面振動によって低い周波数のノイズが感度を汚染する場合があるが、この場合はクロスキャリブレーションのみで使用するの、汚染された周波数を避けてキャリブレーションを行う事が可能であり現実的な使用法と言える。また、復調の必要性について言及する。Pcal を用いて Gcal をキャンセルしているとき、伝達関数は互いに打ち消し合い、最終的に推定される変位およびパワーは周波数によらない。しかし、モータを使用して回転を行った場合、回転の一様性は考慮に入れないといけない。積分を行っている間のドリフトや回転の非一様性は周波数空間上で  $V^R$  を推定する場合に、系統誤差を生じる可能性がある。しかし、エンコーダ信号で Demodulation したシグナルはこれらの効果を含んでいるため、系統誤差を打ち消す事が可能である。したがって、本方法ではでモジュレーションを採用した。

## V. ESTIMATION OF UNCERTAINTY

In evaluating the accuracy of the estimated displacement, we discuss the systematic error by changing the operation frequency and distance. After that, we discuss the uncertainty of the displacement of the mirror. The following discussions are assumed with KAGRA basic parameters ad listed in Table I and parameters of Gcal as listed in Table II. The assumed parameters of the calibrators are listed in Table II. We assumed these number in the following section.

TABLE III. The calculated quadrupole( $N = 2$ ) displacement.  $n$  is order of Legendre polynomial, where  $\omega = n\omega_{\text{rot}}$ .

|    | n=1 | n=2                            | n=3 | n=4   | n=5 | n=6   | n=7 |
|----|-----|--------------------------------|-----|---|-----|---|-----|
| 1f | 0   | 0                              | 0   | 0   | 0   | 0   | 0   |
| 2f | 0   | $9 \frac{Gmr^2}{d^4 \omega^2}$ | 0   | $\frac{25}{4} \frac{Gmr^4}{d^6 \omega^2}$   | 0   | $\frac{735}{128} \frac{Gmr^6}{d^8 \omega^2}$  | 0   |
| 3f | 0   | 0                              | 0   | 0   | 0   | 0   | 0   |
| 4f | 0   | 0                              | 0   | $\frac{175}{16} \frac{Gmr^4}{d^6 \omega^2}$ | 0   | $\frac{441}{64} \frac{Gmr^6}{d^8 \omega^2}$   | 0   |
| 5f | 0   | 0                              | 0   | 0   | 0   | 0   | 0   |
| 6f | 0   | 0                              | 0   | 0   | 0   | $\frac{1617}{128} \frac{Gmr^6}{d^8 \omega^2}$ | 0   |

TABLE IV. The calculated hexapole( $N = 3$ ) displacement.  $n$  is order of Legendre polynomial, where  $\omega = n\omega_{\text{rot}}$ .

|    | n=1 | n=2 | n=3                             | n=4 | n=5   | n=6   | n=7   |
|----|-----|-----|---------------------------------|-----|---|---|---|
| 1f | 0   | 0   | 0                               | 0   | 0   | 0   | 0   |
| 2f | 0   | 0   | 0                               | 0   | 0   | 0   | 0   |
| 3f | 0   | 0   | $15 \frac{Gmr^3}{d^5 \omega^2}$ | 0   | $\frac{315}{32} \frac{Gmr^5}{d^7 \omega^2}$ | 0   | $\frac{189}{64} \frac{Gmr^7}{d^9 \omega^2}$ |
| 4f | 0   | 0   | 0                               | 0   | 0   | 0   | 0   |
| 5f | 0   | 0   | 0                               | 0   | 0   | 0   | 0   |
| 6f | 0   | 0   | 0                               | 0   | 0   | $\frac{4851}{256} \frac{Gmr^6}{d^8 \omega^2}$ | 0   |

### A. Systematic error of the higher order term

In order to achieve the precision less than 1 %, we need to consider the operation position due to the higher order of Legendre polynomial. This is because that higher order also include the 2-f and 3-f components. The  $n$ -th order of the Legendre polynomial is calculated in Eq.(7). The effect of higher order factor is mitigated by the factor of  $(r/d)^n$ . Table III and IV shows the calculated displacement of the higher order term. To compare the higher order effect, we calculate the ratio between the Finite Element Method (FEM) and calculation by changing the  $r/d$  is shown in Fig 5. The results shows that higher the order of polynomials are, the less the systematic errors are. We need to place the mirror at least 2 m away from the mirror and use the sum of first and second order equation to reduce the systematic error. In the following calculation, we assume the distance as 2 m.

### B. Systematic error of the transfer function

The gravity field calibrator can modulate the mirrors with gradient of gravity potential. However, its gravity gradient act the masses of suspension system as shown in Fig. 6. We simulated the transfer function by assuming the cryogenic suspension system in KAGRA [? ]. The transfer function is calculated by the suspension rigid-body simulation code, called SUMCON [? ]. We estimated the total displacement including all the masses. Figure 7 shows the displacement ratio between the sensed motion and free mass motion as a function of frequency. The simulation result is in good agreement with free mass motion at the frequency larger than 10 Hz. The structures of low frequency are corresponding to the resonant

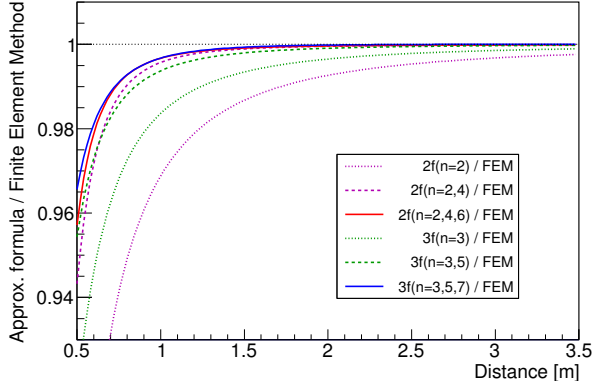


FIG. 5. The displacement ratio of the higher order effect by changing  $r/d$ . Dotted curves are included with the first order term. Dashed curves are included with sum of first order and second order. Solid Curves are assumed with sum of first, second and third order teams. The analytical result is listed in Table III and IV. To achieve the precision less than 1 %, we need to include the higher order terms.

peak of the suspension system. Therefore, we can neglect the intermediate mass effect and regard as free mass motion larger than 10 Hz. On the other hand, we need to consider the elastic deformation [1]. The effect of elastic deformation changes the shape of the mirror and transfer function between the force and displacement due to the mirror position and frequency. However, Gcal dose not generate the elastic deformation because the gravity field act the force to elements mass of the bulk of the test mass uniformly. When we estimate the distance, the difference of the transfer function of Pcal at the 2-f and 3-f generate the systematic error. The estimated displacement ratio is shown as ??, where we assumed Pcal beam position on the mirror is XXXX mm from the center of the mirror surface. Therefore, we need to operate the rotor between 10 Hz and XXX Hz for reducing the error less than 0.1 %. We assumed the rotation frequency as 16 Hz, which is corresponding to 32 Hz and 48 Hz at the operation frequency of 2-f and 3-f components. We used this assumption in the following section.

### C. Uncertainty of displacement and laser power

In this section, we estimate the typical displacement based on the Table. II. We neglect above the second order Legendre polynomial in the following discussion to simplify the discussion. The estimated displacements of

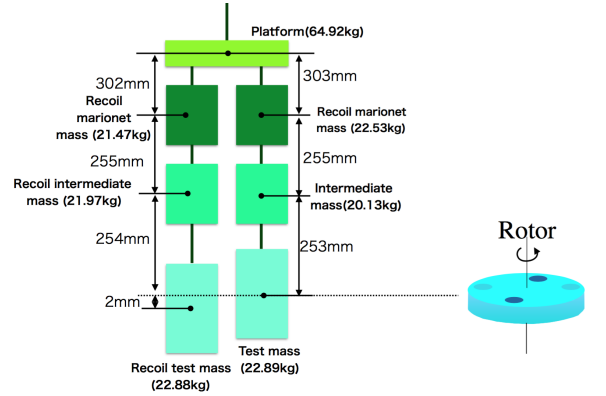


FIG. 6. Schematic view of the suspension system. The parameter of the high and mass is the assumed value.

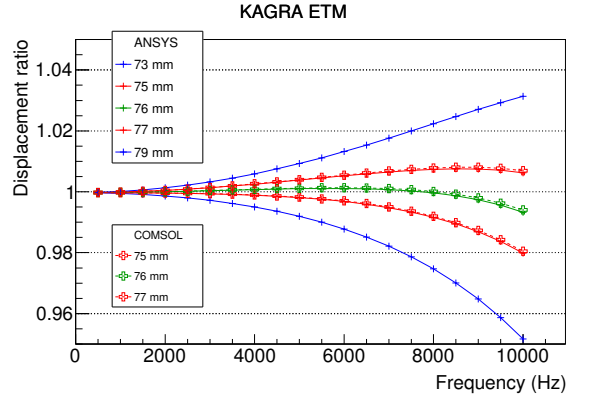


FIG. 7. Estimated elastic deformation of the photon calibrator.

2-f and 3-f are described as

$$x_{2f}^{\text{rms}} = 1.18 \times 10^{-16} [\text{m}] \times \left( \frac{G}{6.67408 \times 10^{-11} [\text{m}^3 \text{kg}^{-1} \text{sec}^{-2}]} \right) \times \left( \frac{m_q}{4.485 [\text{kg}]} \right) \times \left( \frac{r_q}{0.200 [\text{m}]} \right)^2 \times \left( \frac{2 [\text{m}]}{d} \right)^4 \times \left( \frac{2\pi \times 32 [\text{Hz}]}{\omega} \right)^2 \quad (25)$$

$$x_{3f}^{\text{rms}} = 2.13 \times 10^{-18} [\text{m}] \times \left( \frac{G}{6.6742 \times 10^{-11} [\text{m}^3 \text{kg}^{-1} \text{sec}^{-2}]} \right) \times \left( \frac{m_h}{4.485 [\text{kg}]} \right) \times \left( \frac{r_h}{0.125 [\text{m}]} \right)^3 \times \left( \frac{2 [\text{m}]}{d} \right)^5 \times \left( \frac{2\pi \times 48 [\text{Hz}]}{\omega} \right)^2 \quad (26)$$

We define the signal-to-noise ratio ( $SNR$ ) with the ratio of RMS displacement to the design noise spectrum density of IFO of KAGRA at 32 Hz for 2-f and 48 Hz for 3-f. By



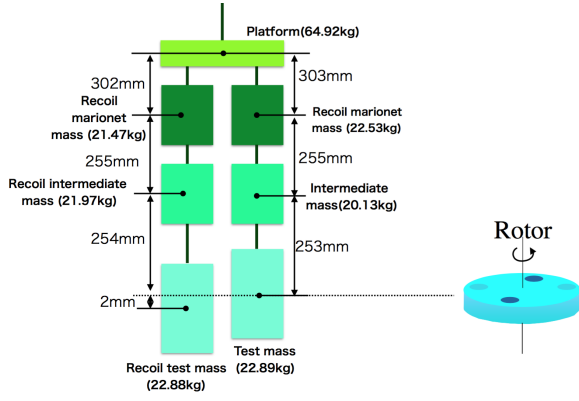


FIG. 8. Schematic view of the suspension system. The parameter of the height and mass is the assumed value.

using this result, we estimate the SNR of the peaks.

$$SNR_{2f} = 392 \times \left( \frac{3.0 \times 10^{-19} [\text{m}/\sqrt{\text{Hz}}]}{n_{32\text{Hz}}} \right) \times \left( \frac{T}{1[\text{sec}]} \right)^{\frac{1}{2}} \times \left( \frac{x_{2f}^{\text{rms}}}{1.178 \times 10^{-16} [\text{m}]} \right), \quad (27)$$

$$SNR_{3f} = 73 \times \left( \frac{2.9 \times 10^{-20} [\text{m}/\sqrt{\text{Hz}}]}{n_{48\text{Hz}}} \right) \times \left( \frac{T}{1[\text{sec}]} \right)^{\frac{1}{2}} \times \left( \frac{x_{2f}^{\text{rms}}}{2.130 \times 10^{-18} [\text{m}]} \right) \quad (28)$$

where  $T$  is integration time. When we integrate the signal larger than 10 min, we can measure the  $V_{2f}^R$  and  $V_{3f}^R$  with enough of SNR. This method are applicable to the measurement of the absolute laser power. The estimated powers are

$$P_{2f} = 0.09288 [\text{W}] \times \left( \frac{G}{6.6742 \times 10^{-11} [\text{m}^3 \text{kg}^{-1} \text{sec}^{-2}]} \right) \times \left( \frac{m_q}{4.485 [\text{kg}]} \right) \times \left( \frac{r_q}{0.200 [\text{m}]} \right)^2 \times \left( \frac{2 [\text{m}]}{d} \right)^4 \times \left( \frac{1}{\cos \theta} \right) \times \left( \frac{1}{1 + \frac{M}{I} \vec{a} \cdot \vec{b}} \right)^2 \quad (29)$$

$$P_{3f} = 0.003779 [\text{W}] \times \left( \frac{G}{6.6742 \times 10^{-11} [\text{m}^3 \text{kg}^{-1} \text{sec}^{-2}]} \right) \times \left( \frac{m_h}{4.485 [\text{kg}]} \right) \times \left( \frac{r_h}{0.125 [\text{m}]} \right)^3 \times \left( \frac{2 [\text{m}]}{d} \right)^5 \times \left( \frac{1}{\cos \theta} \right) \times \left( \frac{1}{1 + \frac{M}{I} \vec{a} \cdot \vec{b}} \right)^2. \quad (30)$$

The estimated  $V_{2f}^T/V_{3f}^T$  by changing distance are shown in Fig. 8. We estimate the laser power by using the following

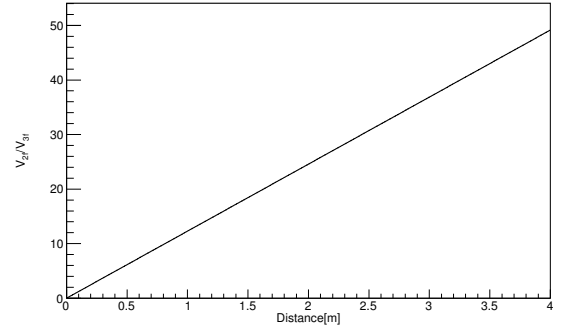


FIG. 9. The response of  $V_{2f}/V_{3f}$  by changing distance between test mass and gravity field calibrator.

equations:

$$\left( \frac{\delta P_{2f}}{P_{2f}} \right)^2 \sim \left( \frac{\delta G}{G} \right)^2 + \left( \frac{\delta M}{M} \right)^2 + \frac{25}{4} \left( \frac{\delta m_q}{m_q} \right)^2 + \frac{16}{6} \left( \frac{\delta m_h}{m_h} \right)^2 + \frac{100}{4} \left( \frac{\delta r_q}{r_q} \right)^2 + \frac{144}{6} \left( \frac{\delta r_h}{r_h} \right)^2 + 16 \left( \frac{\delta V_{2f}^R}{V_{2f}^R} \right)^2 + 16 \left( \frac{\delta V_{3f}^R}{V_{3f}^R} \right)^2 + \left( \frac{\delta \cos \theta}{\cos \theta} \right)^2 + \left( \frac{\delta \left( 1 + \frac{M}{I} \vec{a} \cdot \vec{b} \right)}{\left( 1 + \frac{M}{I} \vec{a} \cdot \vec{b} \right)} \right)^2 \quad (31)$$

$$\left( \frac{\delta P_{3f}}{P_{3f}} \right)^2 \sim \left( \frac{\delta G}{G} \right)^2 + \left( \frac{\delta M}{M} \right)^2 + \frac{25}{4} \left( \frac{\delta m_q}{m_q} \right)^2 + \frac{16}{6} \left( \frac{\delta m_h}{m_h} \right)^2 + \frac{100}{4} \left( \frac{\delta r_q}{r_q} \right)^2 + \frac{144}{6} \left( \frac{\delta r_h}{r_h} \right)^2 + 16 \left( \frac{\delta V_{2f}^R}{V_{2f}^R} \right)^2 + 16 \left( \frac{\delta V_{3f}^R}{V_{3f}^R} \right)^2 + \left( \frac{\delta \cos \theta}{\cos \theta} \right)^2 + \left( \frac{\delta \left( 1 + \frac{M}{I} \vec{a} \cdot \vec{b} \right)}{\left( 1 + \frac{M}{I} \vec{a} \cdot \vec{b} \right)} \right)^2 \quad (32)$$

We consider the mitigation effect of the masses and radiuses due to the tolerance and uncertainty of the measurement instruments. The values of masses and radiuses have a variance due to the fabrication tolerance. The errors of  $m_q$ ,  $r_q$ ,  $m_h$ , and  $r_h$  are mitigated by the factor of  $1/\sqrt{6}$  and  $1/\sqrt{4}$ . Therefore, we divided the factor of these parameter by 4 and 6 in Eq.(31), and (32), respectively. The uncertainty of the quadrupole and hexapole masses are limited by the accuracy of an electronic balance. In this case, we use the masses made of Tungsten. The density of Tungsten is  $19.25 \text{ g/cm}^3$ . The diameter and thickness of mass are 0.06 m and 0.08 m, respectively. Therefore, the mass of the rotor mass is 4.485 kg. To measure this mass, we assumed that we use an electronic balance whose catalog number and accuracy are CG-6000 and 0.2 g, respectively. Therefore, the relative uncertainty of the mass of rotor mass is 0.04 %.

To make the rotor disk, we use the NC milling machine. The typical accuracy is less than 0.02 mm. For the measuring of the shape, we employ the three-dimension coordinate measuring machine (CMM) [? ]. The precision of CMM is  $2 \mu\text{m}$ . We can measure the shape of the rotor and masses with enough of uncertainty using

CMM.

The estimated relative uncertainties of the powers are 0.40 %. One of the largest uncertainties is the geometrical factor of the Pcal laser. The geometrical factor uncertainty is assumed 0.22 %, which is same number of LIGO.

Finally, the estimated relative uncertainty of displacement is written as

$$\begin{aligned} \left(\frac{\delta x}{x}\right)^2 &\sim \left(\frac{\delta G}{G}\right)^2 + \left(\frac{\delta V_{in}}{V_{in}}\right)^2 + \left(\frac{\delta M}{M}\right)^2 + \left(\frac{\delta s(\omega)}{s(\omega)}\right)^2 \\ &+ \frac{25}{4} \left(\frac{\delta m_q}{m_q}\right)^2 + \frac{16}{6} \left(\frac{\delta m_h}{m_h}\right)^2 + 25 \left(\frac{\delta V_{2f}^R}{V_{2f}^R}\right)^2 \\ &+ 16 \left(\frac{\delta V_{3f}^R}{V_{3f}^R}\right)^2 + \frac{100}{4} \left(\frac{\delta r_q}{r_q}\right)^2 + \frac{144}{6} \left(\frac{\delta r_h}{r_h}\right)^2, \quad (33) \end{aligned}$$

where we assumed the mitigation factors of radiuses and masses. The contribution of the radius uncertainty is amplified by the  $O(100)$  factor. To reduce the noise of the displacement, we need to reduce the uncertainty of the shape of the rotor and masses. The uncertainty of the  $V_{2f}^R, V_{3f}^R, V_0^R$  are much less than that of other contributions. We can reduce the uncertainty of these values with long time integration time due to the statistics. Each the uncertainty is listed in Table. II. The estimated total uncertainty of the displacement is 0.22 %.

## VI. CONCLUSION

Photon calibrator is one of the powerful calibrators in advanced LIGO, advanced Virgo and KAGRA. It can calibrate the response of IFO and its uncertainty is essential for estimation of parameters of the gravitational wave source. In particular, the distance of the source is strongly depend on the absolute laser power of the photon calibrator. In previous study, the Gold standard, which response is calibrated by the laser power standard of NIST, is used for the absolute laser power calibration of the photon calibrator. However, current limit of the absolute laser power between each country is about 3.5 %. It is directly propagate to the uncertainty of absolute displacement of the gravitational wave detector.

To solve the problem, we proposed the combination method of the photon calibrator and gravity field calibrator. Gravity field calibrator can modulate the mirror using dynamic gravity field. By canceling the displacement

of the test mass displacement using the photon calibrator, we can calibrate the absolute laser power using gravity field calibrator.

This method has an advantage of a direct comparison of the amplitude of the injected power and gravity field. In previous study, we need to consider the uncertainty of the optical efficiency through the window and mirrors and geometrical factor of the laser position. This is because we put the Working standard at the outside of the chamber. However, the method of gravity field can compare the displacement directly. By using this method, we can calibrate the uncertainty of optical efficiency and absolute power of the laser. The estimated uncertainty of the power of this method is 0.40 %. It imply that we can make a new power standard using interferometer with 10 times improvement.

Finally, we estimate the uncertainty of the absolute calibration. The estimated absolute uncertainty of the displacement is 0.22 %, witch is 10 times better than that of previous study. This uncertainty impact on the estimation of the distance of the gravitational wave source. Of particular importance is that the estimated uncertainty can leach the precision of Hubble constant less than 1 %. It may solve the tension problem between Cepheid-SN distance ladder [?] and CMB data assuming a  $\Lambda$ CDM model [?].

## ACKNOWLEDGMENTS

We thank Richard Savage, Darkhan Tuyrnbayev for discussion of the photon calibrator. We would like to express our gratitude to Prof.Takaaki Kajita and Prof.Henry Wong. We would like to thank the KEK Cryogenics Science Center for the support. YI and SH are supported by Academia Sinica and Ministry of Science and Technology (MOST) under Grants No. CDA-106-M06, MOST106-2628-M-007-005 and MOST106-2112-M-001-016 in Taiwan. This work was supported by JSPS KAKENHI Grant Numbers 17H106133 and 17H01135. KAGRA project is supported by MEXT, JSPS Leading-edge Research Infrastructure Program, JSPS Grant-in-Aid for Specially Promoted Research 26000005, MEXT Grant-in-Aid for Scientific Research on Innovative Areas 24103005, JSPS Core-to-Core Program, A. Advanced Research Networks, and the joint research program of the Institute for Cosmic Ray Research, University of Tokyo.